Article

Understanding type 3 deiodinase on metabolic dysfunction associated fatty liver disease (MAFLD): role on Mitochondria and Krebs Cycle function

Rafael Aguiar Marschner[1], Ana Cristina Roginski[3], Rafael Teixeira Ribeiro[3], Larisse Longo[4,5], Laura Bainy Rodrigues de Freitas[4,5], Mário Reis Álvares-da-Silva[4,5] and Simone Magagnin Wajner[1,2,*].

[1] Endocrine Division, Hospital de Clínicas de Porto Alegre, Universidade Federal do Rio Grande do Sul, Porto Alegre, Rio Grande do Sul, Brazil.
[2] Department of Internal Medicine, Universidade Federal do Rio Grande do Sul (UFRGS), Porto Alegre, RioGrande do Sul, Brazil.
[3] Post-Graduate Program in Biochemestry, Universidade Federal do Rio Grande do Sul (UFRGS), Porto Alegre, RS, Brazil.
[4] Post-Graduate Program in Gastroenterology and Hepatology, Universidade Federal do Rio Grande do Sul, Porto Alegre, Brazil
[5] Experimental Laboratory of Hepatology and Gastroenterology, Center for Experimental Research, Hospital de Clínicas de Porto Alegre, Porto Alegre, Brazil.
* Correspondence: author: E-mail: simone.wajner@ufrgs.br
Disclosure Statement: The authors have nothing to disclose.

Abstract: Metabolic dysfunction associated fatty liver disease (MAFLD) has gained worldwide attention as a public health problem. Nonetheless, lack of enough mechanistic knowledge restrains effective treatment. It is known that thyroid hormone triiodothyronine (T3) regulates hepatic lipid metabolism, and mitochondrial function. Liver dysfunction of type 3 deiodinase (D3) contributes to MAFLD, but its role is not fully understood. Objective: To evaluate the role of D3 in MAFLD in an animal model. Methodology: Male/adult Sprague Dawley rats (n=20) were allocated to a control group (2.93kcal/g) and high-fat diet group (4.3kcal/g). Euthanasia took place in the 28th week. D3 activity and expression, uncoupling protein 2 (UCP2) and type 1 deiodinase (D1) expression, oxidate stress status, mitochondrial, Krebs cycle and endoplasmic reticulum homeostasis were measured in liver tissue. Results: We observed increased D3 activity/expression ($P<0.001$) related to increased thiobarbituric acid reactive substances (TBARS) and carbonyls and diminished reduced glutathione (GSH) in the MAFLD group ($P<0.05$). There was a D3-dependent decrease in UCP2 expression ($P=0.01$), mitochondrial capacity, respiratory activity with increased endoplasmic reticulum stress in the MAFLD group ($P < 0.001$). Surprisingly, in an environment with lower T3 levels due to high D3 activity we observed an augmented alpha-ketoglutarate dehydrogenase (KGDH) and glutamate dehydrogenase (GDH) enzymes activity ($P<0.05$). Conclusion: Induced D3, triggered by changes in the REDOX state, decreases T3 availability, and hepatic mitochondrial capacity. The Krebs cycle enzymes were altered as well as reticulum stress. Taken together, these results shed new light on D3 metabolism in MAFLD.
Keywords: thyroid metabolism; Krebs cycle; MAFLD

1. Introduction

Metabolic dysfunction associated fatty liver disease (MAFLD) is the most common form and the leading cause of morbidity and mortality among liver diseases [1]. The prevalence of MAFLD is around 25-38% of the world population [2, 3]. Although the risk factors associated with the disease and its behavior are well described in the literature, the physiological mechanisms involved in the progression are still unclear [4]. The early stages of the disease are characterized by the accumulation of fat in the liver and chronic inflammation [5]. There are other mechanisms less studied in the understanding of the disease, as T3 regulation, which affect signaling pathways, subsequently altering the

Preprints (www.preprints.org) | NOT PEER-REVIEWED | Posted: 6 December 2022 doi:10.20944/preprints202212.0091.v1

induction of gene and protein expression during progression to other stages of the disease [6].

Thyroid hormones (THs) are essential for growth, development, and metabolism. While thyroxine (T4) is the main product of the thyroid, the biologically active hormone is triiodothyronine (T3). Both THs enter cells via specific transporters and are regulated locally, inside each tissue, by the activity of types 1 (D1), 2 (D2) and 3 (D3) deiodinases. Deiodinases D1 and D2 convert intracellular T4 to T3 [7], while D3 converts T3 to rT3 and other inactive forms [8]. Type 3 deiodinase is known to be augmented in several types of disease, leading to altered local T3 amount in several tissues, as heart and muscle [9, 10]. In the liver, THs directly influence the metabolism of lipids and carbohydrates, through the processes of hepatic lipogenesis, lipid oxidation, cholesterol homeostasis and gluconeogenesis [11-13]. It is known that in the most severe stages of MAFLD, the liver tissue presents a reduction in lipolysis and, consequently, compromises the metabolism of triglycerides and the β-oxidation of free fatty acids (FFAs). Interestingly, the parameters compromised improve with an increase in the availability of T3, reorganizing the hepatic network, mitochondrial turnover, and hepatic autophagy [14, 15].

Type 3 deiodinase directly alters local T3 availability through inflammation and altered oxidative status, thus putatively modifying mitochondrial function, Krebs cycle and endoplasmic reticulum stress. This study aimed to evaluate how D3 dysfunction is associated with these organelle alterations in an animal model of MAFLD.

2. Materials and Methods

2.1. Animals and procedures

Male Sprague Dawley rats (weighing between 250-350g) were used in the experiments. All procedures and experiments involving animals followed the recommendations of the Brazilian College of Animal Experimentation (COBEA). Our study followed the ethical principles of the Guide for the Care and Use of Laboratory Animals [16] and the Guidelines for Reporting Animal Research international standards for animal research [17]. The Research Ethics Committee of our institution and the Animal Ethics Committee of the Hospital de Clínicas de Porto Alegre approved this study (Protocol nº 2019-0297). Briefly, all animals received standard chow or high-fat choline-deficient diet (HFCD) (Rhoster Ltda – Brazil) and water ad libitum throughout the experiment. They were maintained in a 12-hour sleep/wake cycle, at a temperature of 22 ± 1ºC and with air exhaustion.

The experimental model was carried out in accordance with previous studies [18]. A total of 20 rats were allocated into two groups: Control group (n=10) received a standard diet 2.93 kcal/g for 28 weeks and MAFLD group (n=10) received a choline-deficient hyperlipidic diet 4.3 kcal/g (31.5% lipids, enriched with 54.0% trans fatty acids) for 28 weeks. At the end of the experimental period, the animals were sacrificed (anesthetized with a vaporizer (Surgivet, Saint Louis, MN, USA)) and the liver removed, frozen in liquid nitrogen and stored at -80°C.

2.2. Biochemical Parameters

Serum analyzes of triglycerides, total cholesterol, high-density lipoprotein (HDL), low-density lipoprotein (LDL), glucose was measured.

2.3. Hepatic histology and Immunofluorescence

Liver tissue samples were fixed in formalin and embedded in paraffin, later stained with hematoxylin and eosin (H&E) and picrosirius, performed according to the score by Liang et al. [19]. Assessment of the degree of steatosis was performed by a pathologist blinded to the experimental groups. Fibrosis was quantified by morphometric analysis from picrosirius staining. Ten photos of randomly selected fields were obtained per animal, using the Olympus BX51 microscope, QCapture X64 program with 200X magnifi-

 doi:10.20944/preprints202212.0091.v1

cation to determine the labeling intensity. This evaluation was performed using the ImageJ program (version 1.51p).

The immunofluorescence technique was performed according to Solari et al. 2020 [20], with some modifications. Briefly, liver samples fixed in 10% buffered formalin and embedded in paraffin were microtome cut at 3 μm, placed on sialinized slide and deparaffinized. Protein blocking was performed with 3% BSA for 1 hour at room temperature. Slides were permeabilized with 0.05% Tween 20 diluted in PBS. The incubation with the primary antibodies was overnight at 4ºC, the dilutions used were D3 (NBP1-05767, novusbio) 1:400. Incubation with secondary antibody was performed for 1h 30 min at room temperature with anti-rabbit IgG secondary antibody (A11008, Invitrogen-Thermo Fischer), at 1:1000 dilution. The blades were mounted with Fluoroshield mounting medium with Dapi Abcam (ab104139).

2.4. Inflammatory markers

The detection of inflammatory markers was performed using the ELISA technique. Serum concentrations of IL-6 and TNF-α (Invitrogen, USA) were evaluated according to the manufacturer's instructions. All analyzes were performed in duplicate. The absorbance was measured in a spectrophotometer at a wavelength of 450nm (Zenyth 200rt). Results were expressed in pg/mL.

2.5. Oxidative stress parameters

2.5.1. Carbonyl content

Carbonyl content was measured according to Zannata et al. (2013) [21]. The difference between the samples treated with 2,4-dinitrophenylhydrazine and treated with HCl (white) were used to calculate the carbonyl content determined at 370nm. The data obtained were calculated by the millimolar absorption coefficient of hydrazine (e370nm = 21.000000.M-1.cm-1), and the results were expressed in nmol carbonyl/mg of protein.

2.5.2 Malondialdehyde levels

The technique to assess MDA concentrations was based on the method of Yagi (1998) [22]. The fluorescence of the organic phase was read at wavelengths of 515 and 553nm of excitation and emission, respectively. A calibration curve was performed with 1,1,3,3-tetramethoxypropane and subjected to the same treatment as the supernatant. MDA levels were calculated as nanomoles MDA/mg protein.

2.5.3 Sulfhydryl content

The sulfhydryl content was determined as described by Aksenov and Markesbery (2001) [23], where 5-thio-2-nitrobenzoic acid (TNB) derived from the reaction of thiols with 5,5'-dithiobis (2-nitrobenzoic acid) forms a yellow-colored derivative that is read in a spectrophotometer, measuring the absorbance at 412nm. Results were expressed as nmol TNB/mg protein.

2.6. Antioxidant defenses

2.6.1. Reduced glutathione concentrations

The GSH parameter was measured as described by Browne and Armstrong (1998) [24]. Fluorescence was measured using excitation and emission wavelengths of 350 and 420 nm, respectively. The calibration curve was prepared with standard GSH (0.001–1 mM) and concentrations were calculated as nanomoles of GSH/mg protein.

2.6.2. Glutathione peroxide activities

The glutathione peroxidase (GPx) assay was performed according to Wendel (1981) [25]. Enzyme activity was determined by monitoring the disappearance of NADPH at

Preprints (www.preprints.org) | NOT PEER-REVIEWED | Posted: 6 December 2022 doi:10.20944/preprints202212.0091.v1

340nm. The unit of GPx (U) was defined as 1µmol of NADPH consumed per minute. Specific activity was calculated as U/mg of protein.

2.6.3. Glutathione reductase activities

The glutathione reductase (GR) activity was performed according to Carlberg and Mannervik (1985) [26]. Enzyme activity was determined by monitoring NADPH consumption at 340nm. One GR U is defined as 1µmol of GSSG reduced per minute. Specific activity was calculated as U/mg of protein.

2.6.4. Superoxide dismutase activities

Superoxide dismutase (SOD) activity was performed according to the study by Marklund (1985) [27]. The absorbance was read at 420 nm. A calibration curve with purified SOD as a standard was used to calculate the SOD activity present in the samples. Specific activity was calculated as U/mg of protein.

2.7. Real-time PCR

Total RNA was extracted from tissues by the trizol method, cDNA was synthesized (SuperScript First-Strand Synthesis System for RT-PCR; Invitrogen), followed by real-time PCR with SYBR Green PCR Master Mix (Applied Biosystems) in ABI Prism 7500 Sequence Detection System Assay (Applied Biosystems). The r2 was greater than 0.99 and the amplification efficiency varied between 80% and 100%. Samples were measured by relative quantification (change in expression in MAFLD vs Control group).

The oligonucleotides used are described in Table 1:

Primers	***Foward***	***Reverse***
D1	5′-ATTTGACCAGTTCAAGAGACTCGTAG-3′	5′-GGCGTGAGCTTCTTCAATGTA-3′
D3	5'-TTCCAGAGCCAGCACATCCT-3'	5'-ACGTCGCGCTGGTACTTAGTG-3'
Ucp2	5'-TCAACTGTACTGAGCTGGTGACCTA-3'	5'-GGAGGTCGTCTGTCATGAGGTT-3'
Ciclofilin A	5'-GTCAACCCCACCGTGTTCTTC-3'	5'-ACTTGCCACCAGTGCCATTATG-3'

2.8. Mitochondrial capacity

2.8.1. Mitochondrial respiratory parameters (oxygen consumption)

The rate of oxygen consumption was measured using an OROBOROS Oxygraph-2k (Innsbruck, Austria) in a thermostatically controlled (37 °C) and magnetically stirred incubation chamber [28], with modifications [29]. The assay was performed with crude liver homogenates (1 mg tissue.mL -1) and incubated in MIR 05 buffer containing 0.5 mM EGTA, 3 mM MgCl 2 , 60 mM K-lactobionate, 20 mM taurine, 10 mM KH 2 PO 4 , 20 mM HEPES, 110 mM sucrose, 1 g/L BSA, pH 7.1.

Oxygen consumption was measured through substrate-uncoupler inhibitor titration (SUIT) protocol [28]. Oxidative phosphorylation (OXPHOS) capacity (state 3 respiration) was determined by NADH-linked substrates (5 mM pyruvate, 0.5 mM malate, and 10 mM glutamate (PMG) followed by 1 mM ADP to determine the "State 3 – PMG". Following the protocol, the "State 3 – PMG +S" was obtained by supplementation of 10 mM succinate (FADH 2 -linked substrate). Oligomycin (1 µg mL −1) was used to obtain the resting respiration "State 4". Next, 1.5 µM CCCP (three pulses of 0.5 µM) was supplemented to induce the noncoupled respiration "Noncoupled respiration PMG + S", and 2 µM rotenone (complex I inhibitor) was used to obtain the noncoupled respiration stimulated by succinate "Noncoupled respiration S". Finally, 2.5 µM antimycin A (complex III inhibitor) was used to inhibits the transfer of electrons from heme b H to oxidized Q, and with this to block all remaining mitochondrial respiration. The real-time oxygen fluxes were calculated using DatLab7 (Oroboros Instruments) and expressed as pmol O 2 flux·s -1 ·mg protein -1 .

Preprints (www.preprints.org) | NOT PEER-REVIEWED | Posted: 6 December 2022 doi:10.20944/preprints202212.0091.v1

2.8.2. Complexes II, II-III and IV

The liver was homogenized (1:10 w/v) in SETH buffer pH 7.4, centrifuged at 800g for 10min at 4°C and the supernatant was aliquoted and subjected to three cycles of freezing and thawing to rupture the mitochondrial membranes. Afterwards, it was used to determine the activity of the electron transport chain complexes: Complex II–III, analyzed through the reduction of cytochrome C at 550nm [30]; Complex IV, evaluated through the oxidation of cytochrome C at 550nm [31]; and Complex II, evaluated by the determination of succinate-2,6-dichloroindo-phenol (DCIP)-oxidoreductase activity in 600nm [31]. The absorbance variation was detected by a Spectramax M5 microplate spectrofluorometer and the activities of the complexes were calculated, and data expressed as nmol.min− 1.mg protein−1.

Activities of glutamate dehydrogenase (GDH), α-ketoglutarate dehydrogenase (α-KGDH) and succinate dehydrogenase (SDH)

The activities of GDH [32] and α-KGDH [33] were determined by a Spectramax M5 microplate spectrofluorometer using crude liver homogenate (GDH: 0.15mg protein mL−1; α-KGDH: 0.25mg protein mL−1). The activity of both enzymes was determined through the reduction of NAD+ and expressed as nmol.min−1.mg protein−1. The SDH activity [31] was measured using liver homogenate (0.15mg protein mL−1), and the reduction of 2,6-dichloroindophenol (DCIP) at 600 nm, data expressed as nmol.min− 1.mg protein−1.

2.9. Western Blot Analyses

Liver samples were prepared as described by Fuziwara & Kimura (2014) [34]. Briefly, 30-50µg of protein from each sample was fractionated by 8-12% SDS-PAGE and transferred to an Immobilon PVDF membrane (Millipore, Billerica, MA, USA). The following primary antibodies were used: anti-D3 (1:1000; Novus Biologicals); anti-ERK1 (1:500; Santa Cruz Biotechnology); anti-MAPK (1:1000; Cell Signaling Technology); anti-p38 (1:1000; Cell Signaling Technology); anti-GRP78 (1:700; abcam) and anti-β-actin (1:25000; Sigma–Aldrich). Antigen-antibody complexes were visualized using HRP-conjugated secondary antibody and an enhanced chemiluminescence system (GE Healthcare, Pittsburgh, PA, USA). Expression was quantified using image densitometry with ImageJ analysis software.

2.10. D3 activity

The D3 activity of liver samples was determined using the paper chromatography technique as described by Huang et al. (2005) [35]. Briefly, tissues were homogenized and sonicated with 10mM Tris-HCl, 0.25 sucrose buffer (pH 7.5) and 10mM dithiothreitol (DTT). The amount of protein was measured by the Bradford assay. Homogenized livers were incubated for one hour with 200,000 cpm of ^{125}I-labeled T3, 2nM T3, 20mM DTT and 1mM propylthiouracil (PTU) to inhibit any D1 activity. The addition of 200nM of T3 completely abolished D3 activity in all samples. The reaction was stopped with 200µL of 95% ethanol, 50µL of NaOH (0.04N) and 5mg of PTU. Deiodination was determined based on the amount of 125 I-3,3'-T2 generated. Results were expressed as the fraction of T2 counts minus nonspecific deiodination (always <1.5%), obtained with the saturating concentration of T3 (200nM). D3 activity data were expressed as T3 femtomoles per minute per milligram of protein.

2.11. Statistical analysis

Unless otherwise specified, results are presented as mean ± SD. Data were analyzed using 2-tailed Student's t test or 1-way ANOVA followed by post-hoc Duncan multiple-range tests when F was significant. Prism 9.0 software was used for statistical analysis; a P value less than 0.05 was considered significant.

3. Results

Preprints (www.preprints.org) | NOT PEER-REVIEWED | Posted: 6 December 2022 doi:10.20944/preprints202212.0091.v1

3.1. Sample characteristics and biochemical parameters

The body weight of animals in the MAFLD group was significantly higher compared to their control (P<0.01). The biochemical parameters were altered in the MAFLD group regarding serum levels of glucose (P<0.05), triglycerides (P<0.05), LDL cholesterol (P<0.05) and total cholesterol (P<0.05, Table 2).

Table 2: Biochemical data at the end of the experiment

Variables	Control	MAFLD	P Value
Weight (g)	535,5 (±45,14)	644,2 (±42,15)	<0.01
Glucose (mg/dl)	278,2 (±56,76)	353,4 (±64,30)	<0.05
Triglycerides (mg/dl)	79,33 (±14,71)	105,6 (±23,71)	<0.05
LDL cholesterol (mg/dl)	16,65 (±2,74)	23,41 (±6,63)	<0.05
HDL cholesterol (mg/dl)	53,23 (±9,77)	31,27 (±6,63)	<0.01
Total cholesterol (mg/dl)	78,74 (±11,72)	101,8 (±27,54)	<0.05

3.2. MAFLD generates histopathological changes

Animals in the control group did not show any type of abnormality in the liver tissue (Fig. 1A), whether animals in the MAFLD group presented moderate intensity microvesicular and macrovesicular steatosis, in addition to a mild degree of fibrosis (Fig. 1B). Collagen quantification showed a significantly higher amount of connective tissue fibers (P<0.01) in the MAFLD group compared to the control group (Fig. 1C).

Preprints (www.preprints.org) | NOT PEER-REVIEWED | Posted: 6 December 2022 doi:10.20944/preprints202212.0091.v1

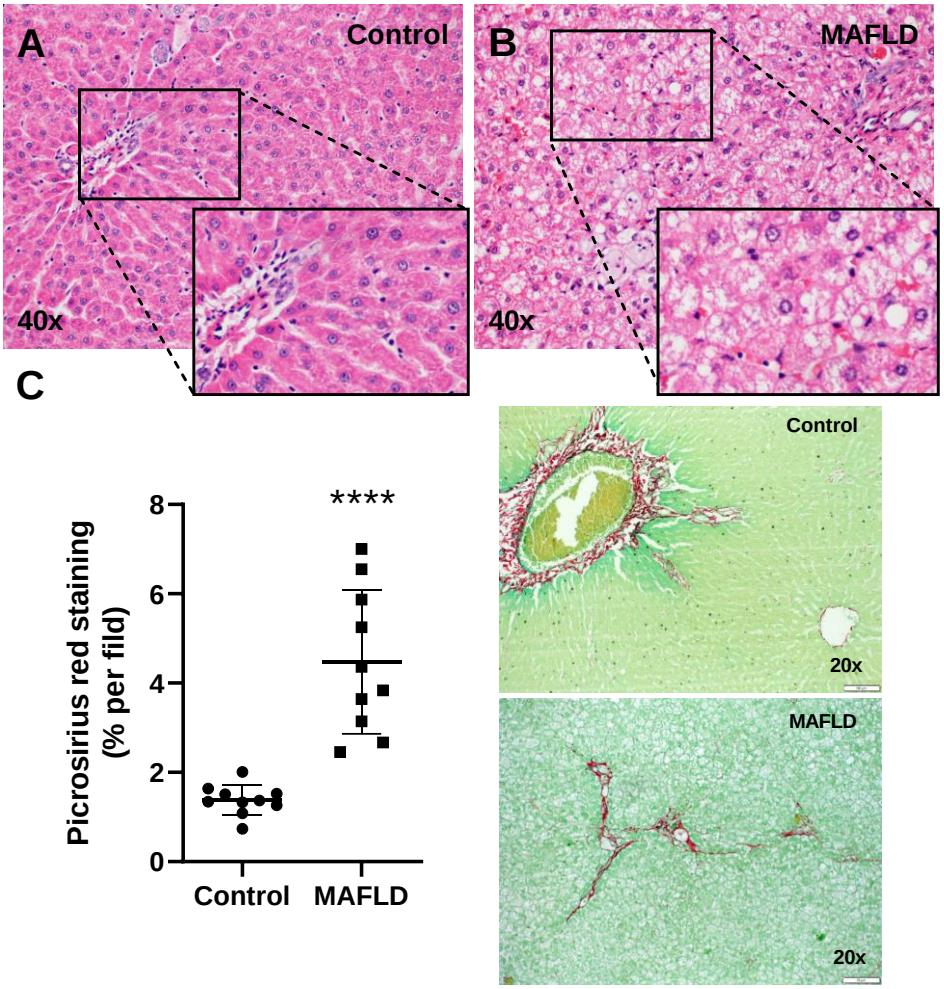

Figure 1. Histological evaluation of the liver. Control (A) and MAFLD (B) groups, H&E staining, at 40x magnification. Assessment by Picrosirius (C), the MAFLD group showed an increase for fibers. ** P<0.01 vs Control, n=10 per group.

3.3. Changes in inflammatory and REDOX state parameters are induced by MAFLD

The hepatic concentrations of the pro-inflammatory cytokines IL-6 (P<0.05) and TNF-α (P<0.01) were significantly higher in the MAFLD group when compared to the control (Fig. 2A). The protein and lipid damage assessments in liver tissue were performed with Carbonyl and MDA assays, respectively. Carbonyl and TBARS (P<0.001) were increased in the MAFLD group related to controls (Fig. 2B). Reduced GSH levels (P<0.01) were present in MAFLD animals, which might suggest an increase in reactive oxygen species induced by HFCD (Fig. 2C). The activity of GPx (P<0.05) was increased in the MAFLD group, the same observed in the activity of GR (P<0.01) and SOD (P<0.05) enzymes (Fig. 2C).

Preprints (www.preprints.org) | NOT PEER-REVIEWED | Posted: 6 December 2022 doi:10.20944/preprints202212.0091.v1

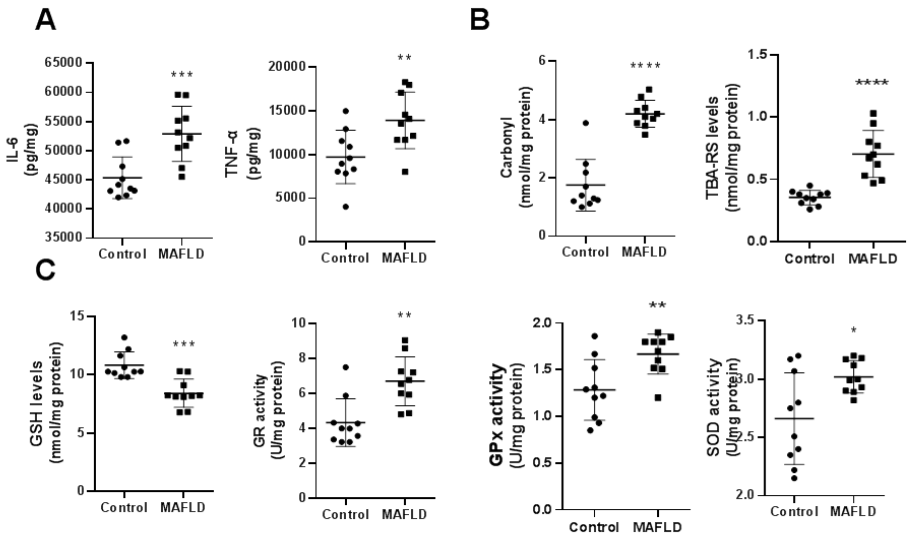

Figure 2. Evaluation of inflammatory markers, IL-6 and TNF-α, in the liver (Panel A). The quantification of IL-6 and TNF-α were shown to be increased in the MAFLD group. As for the REDOX state, we evaluated the content of carbonyl groups and TBA (Panel B) and levels of GSH, GPx, GR and SOD activity (Panel C) in the liver. The carbonyl and TBA increased content in the MAFLD group (B). GSH content was decreased in liver samples from MAFLD animals (C), while GPx, GR and SOD activity were increased in the MAFLD group (C). *P<0.05; **P<0.01; ***P< 0.001 vs Control, n=10 in each group.

3.4. Altered mechanisms of thyroid hormone metabolism in MAFLD

We then determined the expression and activity, in the liver, of type 3 deiodinase (D3), the key enzyme in the inactivation of T3 that is usually altered in disease. There was a significant increase in its expression, and D3 activity (P<0.0001) in MAFLD animals (Fig. 3A), representing a higher T3 inactivation. The pathways capable of stimulating the activity of D3 in the liver. While the MAPK pathway was increased in 11%, ERK increased 21% and p38 increased 68% in MAFLD (Fig. 3B). As expected, there was a reduced expression of D1 mRNA and UCP2 mRNA (P<0.0001), genes positively stimulated by T3 hormone activity in the liver of the MAFLD group (Fig. 3C), indicating lower amount of T3 in this organ in MAFLD.

Preprints (www.preprints.org) | NOT PEER-REVIEWED | Posted: 6 December 2022 doi:10.20944/preprints202212.0091.v1

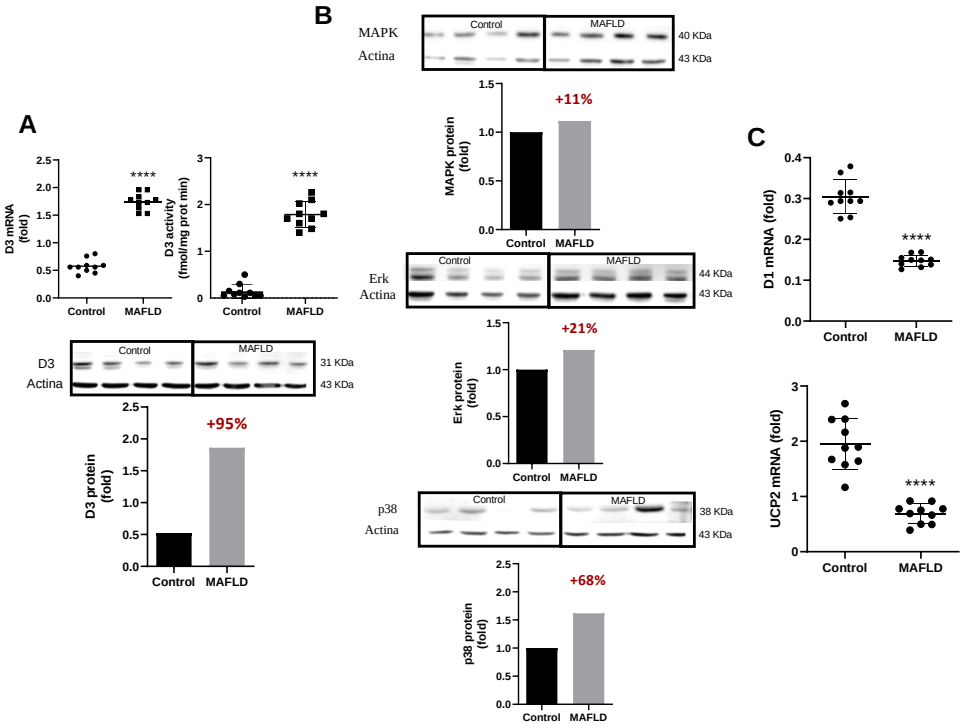

Figure 3. Assessment of thyroid metabolism in the liver (Panel A). D3 mRNA expression, activity and protein quantification showed an increase in MAFLD animals (A). Evaluation of the mechanisms involved with D3 (Panel B). The MAPK pathway showed an increase of 11% in protein quantification, while its subsequent ERK and p38 pathways showed an increase of 21 and 68%, respectively in MAFLD animals. Evaluation of the expression of genes linked or stimulated by the T3 hormone (Panel C). D1 and UCP2 mRNA expression showed a reduction in MAFLD animals (C). ****P< 0.0001 vs Control, n=10 in each group.

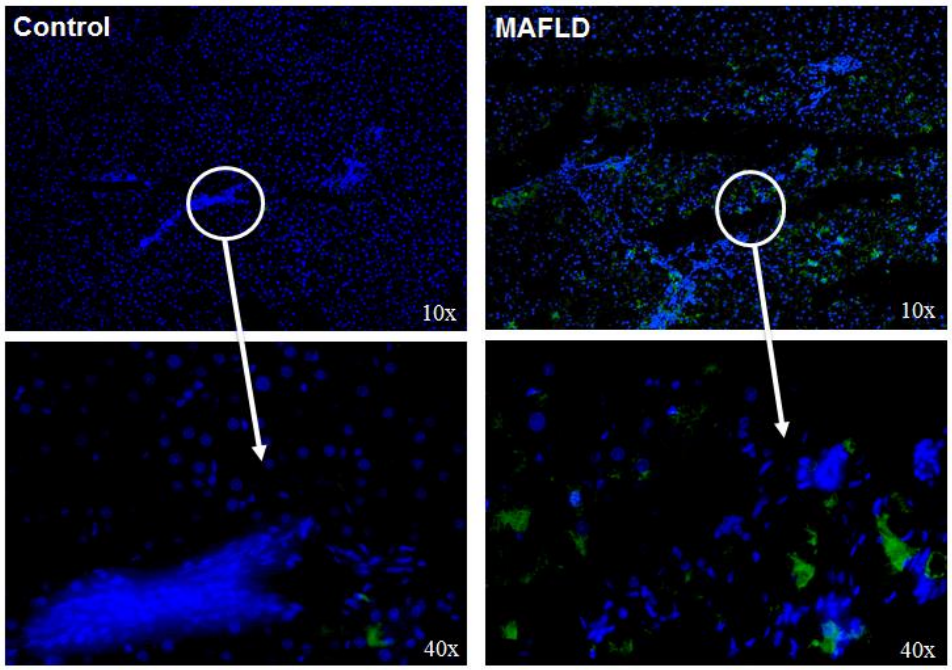

Figure 4. Assessment of thyroid metabolism in the liver. D3 showed immunofluorescence an increase in MAFLD animals.

3.5. Mitochondrial complexes are affected in MAFLD

Preprints (www.preprints.org) | NOT PEER-REVIEWED | Posted: 6 December 2022 doi:10.20944/preprints202212.0091.v1

The complex II and II-III activity were reduced (P<0.0001) as the MAFLD group had lower levels compared to the control group (Fig. 5A). No difference between groups was observed with complex IV activity (P=0.0986, Fig. 5A).

3.6. MAFLD induced impairment of mitochondrial capacity

MAFLD animals showed reduced hepatic respiratory capacity. State 3 capacity (stimulated by PMG) showed a significant decrease (P<0.01) in MAFLD. The same can be observed in state 3 when stimulated by PMG + S and respiration in state 4 (stimulated by oligomycin), demonstrating a reduction (P<0, 01) in the MAFLD group. Finally, the uncoupled states (stimulated by S and by PMG+S) also showed a significant reduction in their respiratory capacity (P<0.0001, Fig. 5B).

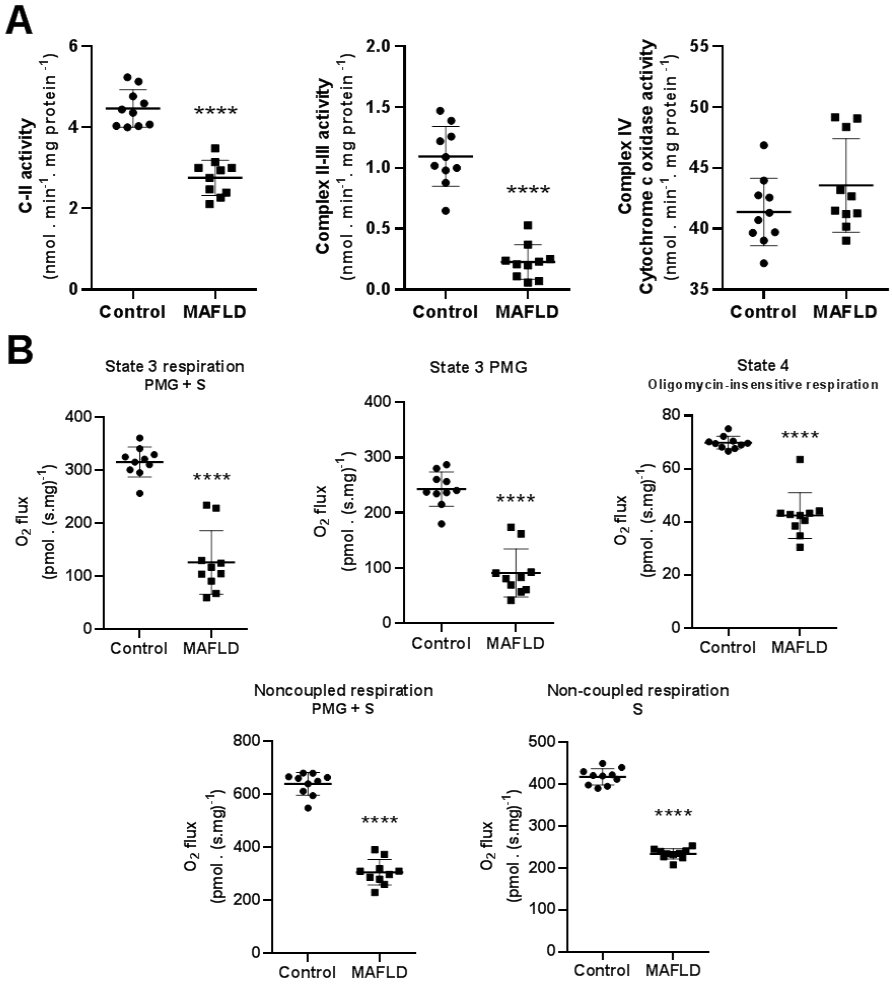

Figure 5. Assessment of mitochondrial respiratory complexes and capacity in the liver. The activity of complexes II and II-III showed a reduction in the MAFLD group, which was not observed in complex IV (Panel A). Liver respiratory capacity was reduced in MAFLD animals, as state 3 (stimulated by PMG and PMG+S) and state 4 (stimulated by oligomycin) breaths showed a decrease (Panel B). The same can be observed in the uncoupled states (stimulated by S and by PMG+S) also showed a reduction (Panel B). **P<0.01; ***P< 0.0001 vs Control, n=10 in each group.

3.7. MAFLD induces GDH, α-KGDH, SDH enzymes and Endoplasmic reticulum stress

The next step was to understand the mechanisms by which HFCD inhibited mitochondrial respiration and reticulum capacity in the liver. We evaluated the effect of HFCD on the enzymes GDH, α-KGDH and SDH, which have great importance in mitochondrial capacity, has a fundamental role in the Krebs cycle in the conversion of α-ketoglutarate to succinyl-CoA by α-KGDH and succinate to fumarate by SDH. The activity of the enzymes GDH and α-KGDH showed an increase (P<0.0001 both) while the

Preprints (www.preprints.org) | NOT PEER-REVIEWED | Posted: 6 December 2022 doi:10.20944/preprints202212.0091.v1

activity of SDH reduced (P<0.0001) in the MAFLD (Fig. 6A). Interestingly, these enzymes are not only correlated with disease worsening, as expected, but also with type 3 deiodinase. Furthermore, when we evaluated the endoplasmic reticulum, we found that the animals induced to MAFLD had a 58% increase in reticulum stress (Fig. 6B).

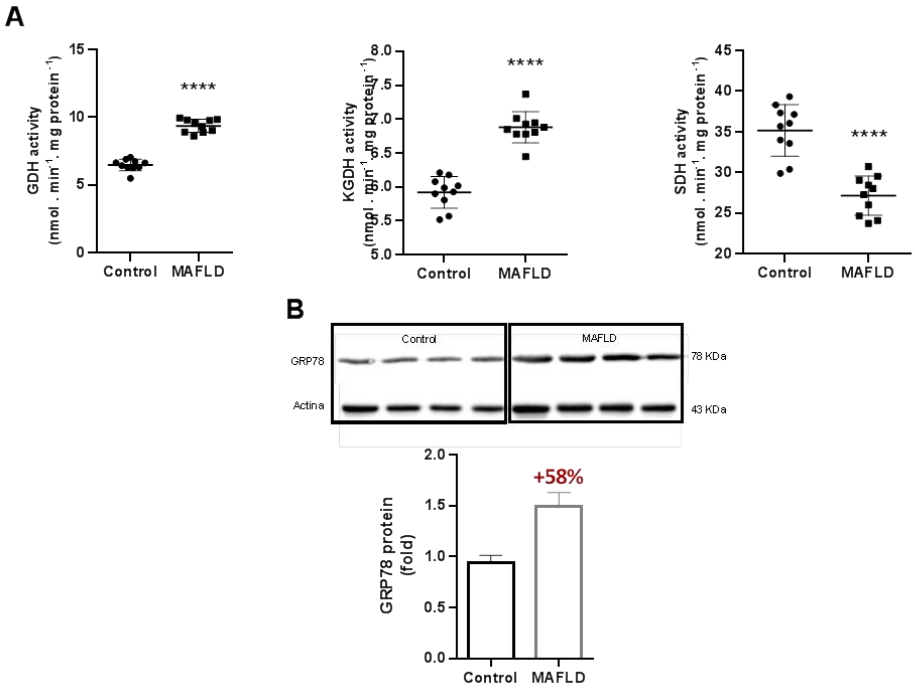

Figure 6. GDH, α-KGDH, SDH activity and GRP78 protein in the liver. The activity of the enzymes GDH and α-KGDH were increased while SDH activity decreases in MAFLD animals (Panel A). GRP78 showed a 58% increase in the MAFLD group compared to the control group (Panel B). ****P<0.0001 vs Control, n=10 in each group.

4. Discussion

The present study examines the type 3 deiodinase effect on T3 levels in the progression of metabolic dysfunction-associated fatty liver disease (MAFLD). The results showed that the accumulation of IL-6, as well as the increase in TBA-RS and carbonyls augments D3 expression and activity. The reduction in GSH and sulfhydryl levels are observed in parallel with increased D3 function in liver tissue. In addition, GPx, GR and SOD enzymes were altered, leaving a pro-oxidative REDOX state. Importantly, UCP2 and Dio1 expressions were low, showing a decrease on local levels of T3. Moreover, while the mitochondrial capacity is diminished, an increase in the GDH and α-KGDH enzymes are observed. Together with high endoplasmic reticulum stress, this set of results add to the current knowledge of type 3 deiodinase and T3 role on MAFLD.

The augmented expression of D3 in MAFLD, so far not explored, leads to a whole cascade of T3 dependent alterations. Previous studies found that changes in the inflammatory profile and oxidation status (REDOX) induce increased D3 activity in acute illness situations [36-38]. Here we observed that in a model of chronic disease, the accumulation of hepatic fat, via high-fat diet, induces inflammatory changes and a consequent increase in the production of reactive oxygen species (ROS) [39-44]. These data reinforce the direct association between the inflammatory profile and the REDOX state with diminished T3 levels, via an increase in D3 activity and a reduction in D1. The interaction between T3 and mitochondria is complex. T3 controls UCP2 and it can act as a transporter for fatty acids, modulating mitochondrial metabolic activity. Moreover, the interaction involving T3 tightly controls Ca^{2+} in the mitochondria membrane as well as its metabolic activity [45, 46]. T3 amount affects the turnover of Krebs cycle, which in turn is strongly dependent on dehydrogenases in the mitochondrial matrix [47]. This been said, the altered D3 activity which speeds T3 inactivation, can be one factor that explains the lower energy

 doi:10.20944/preprints202212.0091.v1

production and the altered electron transport chain in the Krebs cycle, which reduces the respiratory capacity and causes mitochondrial dysfunction in MAFLD.

The results shown here also clarify the data described in recent studies that used THR-β analogues [48, 49]. The study by Caddeo et al. (2021) evaluated the effect of TG68 (new THR-β agonist) in an animal model of MAFLD. The results demonstrate that TG68 increases the sensitivity of THR-β in the liver, increasing the availability of T3 to activate genes linked to the hepatic metabolism such as Acyl-CoA Oxidase-1 (ACOX1) and carnitine palmitoyltransferase-1 (CPT-1) and D1. In addition, TG68 exerts an anti-steatogenic effect, improving 30% of fat liver content [48]. The increase on receptor availability improves liver function and increases metabolism of lipids and lipoproteins [49]. Nevertheless, these agonists alone were able to solve only a part of the whole disease process, suggesting that other adjuvant therapeutics are necessary to stabilize the disease.

In addition, we show that increased D3 tissue activity occurs secondary to the augmented MAPK signaling pathway, via ERK and p38, which are already positively related to the expression and activity of D3 [50]. Here it is demonstrated an expressive augment in the MAPK/ERK/p38 pathway (Fig. 3B). The increased expression in p38 and ERK in MAFLD can be due to increased hypoxia and consequently cellular apoptosis, perpetuating a cycle of metabolic dysfunction in the liver and probably accelerating disease progression [51]. A former report has revealed an inverse correlation between UCP2 mRNA expression and ER-mitochondrial interaction [52]. T3 controls the interaction between mitochondria and ER while UCP2 is augmented [46]. In MALFD we observed the opposite: lower levels of UCP2 probably secondary to lower T3 augments this interaction, resulting in augmented reticulum stress, which can also result in cell apoptosis.

Interestingly, here we can observe an early double harm. T3 regulates the ER-mitochondrial contact interaction, which might alter the function of both organelles. However, whether this event can alter mitochondrial activity is not elucidated. Here we advance in this question showing that the augmented T3 inactivation by D3 can disrupt this interface by altering protein function via disruption of disulfide bonds, for example. In addition, T3 also affect the transport of fatty acid transport [53], as the MAFLD group showed a significant reduction in their respiratory capacity (Fig. 5B). One need to consider a decrease in mitochondrial content [54]. It is known that T3 can stimulate the PGC1-α pathway, an important protein linked to mitochondrial biogenesis [55]. In this sense, the reduction in the availability of T3 as D3 augments its activity, decreases the hepatic mitochondrial content and the capacity of the remaining mitochondria to uncouple properly. These alterations negatively impact the β-oxidation of fatty acids in the liver, accelerating the progression of the disease to other stages.

Finally, proper T3 levels are essential to maintain the activity of dehydrogenases like α-ketoglutarate dehydrogenase of the Krebs cycle [46]. In other words, T3 enables homeostasis and dehydrogenase activity. Interestingly, despite the impairment of the respiratory chains, an increase in the activity of GDH and α-KGDH enzymes was observed in the liver of MAFLD animals (Fig. 5). It is known that the enzymes GDH and α-KGDH, in addition to their energetic function, are of great importance in the urea cycle for ammonia absorption [56]. Translating these results to clinical observations, we know that hyperammonemia is associated with advanced MAFLD. Now we add in knowledge showing that the reduction of T3 availability is a contributing factor in augment its toxicity, forming a continuous damage cycle that culminates, in the long term, in hepatic encephalopathy [57, 58] .

Interestingly, data found here suggest an attempt to increase the deamination system due to the harm generated by excess ammonia already in the early stages of the disease. This might be due to the diminished T3 levels, among other factors. The importance of GDH and α-KGDH in this process was also observed in a hepatic model of GDH-knockout, where hepatic deletion of GDH triggered a systemic increase in ammonia, in response to reduced urea detoxification and increased ammonia production [59]. Moreover, GDH is also released by injured hepatocytes, catalyzing a blood reaction that consumes ammonia and α-KGDH to generate glutamate. This process continues until the

 doi:10.20944/preprints202212.0091.v1

total consumption of α-KGDH in the blood. In this situation, there is a margin of therapeutic opportunity with antioxidants and agents that absorbs ammonia that can bring good results in preventing disease complications [56].

The whole set of these results brings a total new perception of the impact of increased inactivation of the T3 hormone in liver, caused by augmented D3 activity. This new information directly linking D3 in MAFLD may bring new insights at the mechanisms involved in disease, in addition to opening a new window of opportunity in the treatment of MAFLD.

5. Conclusions

Taken together, our findings demonstrate that the deposit of fat in the liver leads to inflammation and imbalance in the REDOX state, resulting in an increase in D3 activity and, inactivation of T3. The lack of T3 leads to mitochondrial dysfunction and, at the same time, an underexplored mechanism for the role of α-KGDH, decreasing as the patient's clinical condition deteriorates. This reduction raises ammonia concentrations, further decreasing the availability of hepatic T3. The ammonia and T3 ratio open a new therapeutic window to correct the increased D3 and its potential tissue damage and complications as hepatic encephalopathy. The set of results suggest a new and very important role of thyroid hormone metabolism in MAFLD progression.

Author Contributions: Conceptualization, S.M.W., M.R.A.S and R.A.M.; Methodology, M.R.A.S., l.l. and l.R.F.; Validation, S.M.W. and M.R.A.S; Formal analysis, R.A.M., A.C.R. and R.T.R.; Investigation, S.M.W.; Resources, S.M.W. and M.R.A.S.; Data curation, S.M.W.; Writing—preparation of the original draft, S.M.W., M.R.A.S and R.A.M.; Writing—review and editing, S.M.W., M.R.A.S and R.A.M.; Supervision, S.M.W.; Project management, S.M.W., M.R.A.S. All authors read and agreed with the published version of the manuscript.

Funding: This research was funded by Coordenação de Aperfeiçoamento de Pessoal de Nivel Superior (CAPES, PROEX, number 88882.346533/2019-01); Fundo de Incentivo a Pesquisa do Hospital de Clínicas de Porto Alegre (FIPE- 20220167 and 20190167), Brazil.

Institutional Review Board Statement: The animal study protocol was approved by The Research Ethics Committee of our institution and the Animal Ethics Committee of the Hospital de Clínicas de Porto Alegre approved this study (Protocol nº 2019-0297).

Informed Consent Statement: Not applicable.

Conflicts of Interest: The authors declare no conflict of interest.

References

1. Francque, S.M., D. van der Graaff, and W.J. Kwanten, *Non-alcoholic fatty liver disease and cardiovascular risk: Pathophysiological mechanisms and implications.* J Hepatol, 2016. **65**(2): p. 425-43.

2. Lazarus, J.V., et al., *Advancing the global public health agenda for NAFLD: a consensus statement.* Nat Rev Gastroenterol Hepatol, 2022. **19**(1): p. 60-78.

3. Chan, K.E., et al., *Global Prevalence and Clinical Characteristics of Metabolic Associated Fatty Liver Disease. A Meta-Analysis and Systematic Review of 10,739,607 Individuals.* J Clin Endocrinol Metab, 2022.

4. Than, N.N. and P.N. Newsome, *A concise review of non-alcoholic fatty liver disease.* Atherosclerosis, 2015. **239**(1): p. 192-202.

5. Day, C.P. and O.F. James, *Steatohepatitis: a tale of two "hits"?* Gastroenterology, 1998. **114**(4): p. 842-5.

 doi:10.20944/preprints202212.0091.v1

6. Hones, G.S., et al., *Noncanonical thyroid hormone signaling mediates cardiometabolic effects in vivo.* Proc Natl Acad Sci U S A, 2017. **114**(52): p. E11323-E11332.

7. Peeters, R.P. and T.J. Visser, *Metabolism of Thyroid Hormone*, in *Endotext*, K.R. Feingold, et al., Editors. 2000: South Dartmouth (MA).

8. Bianco, A.C., et al., *Biochemistry, cellular and molecular biology, and physiological roles of the iodothyronine selenodeiodinases.* Endocr Rev, 2002. **23**(1): p. 38-89.

9. Ogawa-Wong, A., et al., *Modulation of Deiodinase Types 2 and 3 during Skeletal Muscle Regeneration.* Metabolites, 2022. **12**(7).

10. Lehnen, T.E., et al., *Oxidative remote induction of type 3 deiodinase impacts nonthyroidal illness syndrome.* J Endocrinol, 2020. **246**(3): p. 237-246.

11. Raftopoulos, Y., et al., *Improvement of hypothyroidism after laparoscopic Roux-en-Y gastric bypass for morbid obesity.* Obes Surg, 2004. **14**(4): p. 509-13.

12. Sinha, R.A., B.K. Singh, and P.M. Yen, *Thyroid hormone regulation of hepatic lipid and carbohydrate metabolism.* Trends Endocrinol Metab, 2014. **25**(10): p. 538-45.

13. Sinha, R.A., et al., *Thyroid hormone stimulates hepatic lipid catabolism via activation of autophagy.* J Clin Invest, 2012. **122**(7): p. 2428-38.

14. Piantanida, E., et al., *The interplay between thyroid and liver: implications for clinical practice.* J Endocrinol Invest, 2020. **43**(7): p. 885-899.

15. Vallejo, C.G., et al., *Thyroid hormone regulates tubulin expression in mammalian liver. Effects of deleting thyroid hormone receptor-alpha or -beta.* Am J Physiol Endocrinol Metab, 2005. **289**(1): p. E87-94.

16. NIH, *Guide for the Care and Use of Laboratory Animals.* National Academy Press. Washington, DC,. 1996.

17. Kilkenny, C., et al., *Improving bioscience research reporting: The ARRIVE guidelines for reporting animal research.* J Pharmacol Pharmacother, 2010. **1**(2): p. 94-9.

18. Silva, E.P., *Modelo experimental para indução da esteatose hepática e esteatohepatite: estudo em ratos.* Programa de Ciências em Gastroenterologia, Faculdade de Medicina da Universidade de São Paulo., 2012.

19. Liang, W., et al., *Establishment of a general NAFLD scoring system for rodent models and comparison to human liver pathology.* PLoS One, 2014. **9**(12): p. e115922.

20. Solari, J.I.G., et al., *Damage-associated molecular patterns (DAMPs) related to immunogenic cell death are differentially triggered by clinically relevant chemotherapeutics in lung adenocarcinoma cells.* BMC Cancer, 2020. **20**(1): p. 474.

21. Zanatta, A., et al., *Disturbance of redox homeostasis by ornithine and homocitrulline in rat cerebellum: a possible mechanism of cerebellar dysfunction in HHH syndrome.* Life Sci, 2013. **93**(4): p. 161-8.

22. Yagi, K., *Simple procedure for specific assay of lipid hydroperoxides in serum or plasma.* Methods Mol Biol, 1998. **108**: p. 107-10.

23. Aksenov, M.Y. and W.R. Markesbery, *Changes in thiol content and expression of glutathione redox system genes in the hippocampus and cerebellum in Alzheimer's disease.* Neurosci Lett, 2001. **302**(2-3): p. 141-5.

24. Browne, R.W. and D. Armstrong, *Reduced glutathione and glutathione disulfide.* Methods Mol Biol, 1998. **108**: p. 347-52.

 doi:10.20944/preprints202212.0091.v1

25. Wendel, A., *Glutathione peroxidase.* Methods Enzymol, 1981. **77**: p. 325-33.
26. Carlberg, I. and B. Mannervik, *Glutathione reductase.* Methods Enzymol, 1985. **113**: p. 484-90.
27. Marklund, S.L., *Product of extracellular-superoxide dismutase catalysis.* FEBS Lett, 1985. **184**(2): p. 237-9.
28. Gnaiger, E., *Capacity of oxidative phosphorylation in human skeletal muscle: new perspectives of mitochondrial physiology.* Int J Biochem Cell Biol, 2009. **41**(10): p. 1837-45.
29. Roginski, A.C., et al., *Disturbance of bioenergetics and calcium homeostasis provoked by metabolites accumulating in propionic acidemia in heart mitochondria of developing rats.* Biochim Biophys Acta Mol Basis Dis, 2020. **1866**(5): p. 165682.
30. Rustin, P., et al., *Biochemical and molecular investigations in respiratory chain deficiencies.* Clin Chim Acta, 1994. **228**(1): p. 35-51.
31. Fischer, J.C., et al., *Differential investigation of the capacity of succinate oxidation in human skeletal muscle.* Clin Chim Acta, 1985. **153**(1): p. 23-36.
32. Melo, D.R., et al., *Methylmalonate impairs mitochondrial respiration supported by NADH-linked substrates: involvement of mitochondrial glutamate metabolism.* J Neurosci Res, 2012. **90**(6): p. 1190-9.
33. Tretter, L. and V. Adam-Vizi, *Inhibition of Krebs cycle enzymes by hydrogen peroxide: A key role of [alpha]-ketoglutarate dehydrogenase in limiting NADH production under oxidative stress.* J Neurosci, 2000. **20**(24): p. 8972-9.
34. Fuziwara, C.S. and E.T. Kimura, *High iodine blocks a Notch/miR-19 loop activated by the BRAF(V600E) oncoprotein and restores the response to TGFbeta in thyroid follicular cells.* Thyroid, 2014. **24**(3): p. 453-62.
35. Huang, S.A., et al., *Transforming growth factor-beta promotes inactivation of extracellular thyroid hormones via transcriptional stimulation of type 3 iodothyronine deiodinase.* Mol Endocrinol, 2005. **19**(12): p. 3126-36.
36. Lehnen, T.E., et al., *N-Acetylcysteine Prevents Low T3 Syndrome and Attenuates Cardiac Dysfunction in a Male Rat Model of Myocardial Infarction.* Endocrinology, 2017. **158**(5): p. 1502-1510.
37. Vidart, J., et al., *N-acetylcysteine administration prevents nonthyroidal illness syndrome in patients with acute myocardial infarction: a randomized clinical trial.* J Clin Endocrinol Metab, 2014. **99**(12): p. 4537-45.
38. Wajner, S.M., et al., *IL-6 promotes nonthyroidal illness syndrome by blocking thyroxine activation while promoting thyroid hormone inactivation in human cells.* J Clin Invest, 2011. **121**(5): p. 1834-45.
39. Bruinstroop, E., et al., *Low-Dose Levothyroxine Reduces Intrahepatic Lipid Content in Patients With Type 2 Diabetes Mellitus and NAFLD.* J Clin Endocrinol Metab, 2018. **103**(7): p. 2698-2706.
40. Bruinstroop, E., et al., *Early induction of hepatic deiodinase type 1 inhibits hepatosteatosis during NAFLD progression.* Mol Metab, 2021. **53**: p. 101266.
41. Ge, Y., et al., *Oxidized Pork Induces Hepatic Steatosis by Impairing Thyroid Hormone Function in Mice.* Mol Nutr Food Res, 2022. **66**(1): p. e2100602.
42. Grasselli, E., et al., *3,5-diiodo-L-thyronine modifies the lipid droplet composition in a model of hepatosteatosis.* Cell Physiol Biochem, 2014. **33**(2): p. 344-56.
43. Iannucci, L.F., et al., *Metabolomic analysis shows differential hepatic effects of T2 and T3 in rats after short-term feeding with high fat diet.* Sci Rep, 2017. **7**(1): p. 2023.
44. Souza, L.L., et al., *Thyroid hormone contributes to the hypolipidemic effect of polyunsaturated fatty acids from fish oil: in vivo evidence for cross talking mechanisms.* J Endocrinol, 2011. **211**(1): p. 65-72.

 doi:10.20944/preprints202212.0091.v1

45. Denton, R.M., *Regulation of mitochondrial dehydrogenases by calcium ions.* Biochim Biophys Acta, 2009. **1787**(11): p. 1309-16.

46. Tawfik, I., et al., *T3-induced enhancement of mitochondrial Ca(2+) uptake as a boost for mitochondrial metabolism.* Free Radic Biol Med, 2022. **181**: p. 197-208.

47. Cicatiello, A.G., D. Di Girolamo, and M. Dentice, *Metabolic Effects of the Intracellular Regulation of Thyroid Hormone: Old Players, New Concepts.* Front Endocrinol (Lausanne), 2018. **9**: p. 474.

48. Caddeo, A., et al., *TG68, a Novel Thyroid Hormone Receptor-beta Agonist for the Treatment of NAFLD.* Int J Mol Sci, 2021. **22**(23).

49. Harrison, S.A., et al., *Effects of Resmetirom on Noninvasive Endpoints in a 36-Week Phase 2 Active Treatment Extension Study in Patients With NASH.* Hepatol Commun, 2021. **5**(4): p. 573-588.

50. Romitti, M., et al., *Signaling pathways in follicular cell-derived thyroid carcinomas (review).* Int J Oncol, 2013. **42**(1): p. 19-28.

51. Zhou, J., et al., *Thyroid Hormone Decreases Hepatic Steatosis, Inflammation, and Fibrosis in a Dietary Mouse Model of Nonalcoholic Steatohepatitis.* Thyroid, 2022. **32**(6): p. 725-738.

52. Madreiter-Sokolowski, C.T., et al., *Dynamic Control of Mitochondrial Ca(2+) Levels as a Survival Strategy of Cancer Cells.* Front Cell Dev Biol, 2021. **9**: p. 614668.

53. Berardi, M.J. and J.J. Chou, *Fatty acid flippase activity of UCP2 is essential for its proton transport in mitochondria.* Cell Metab, 2014. **20**(3): p. 541-52.

54. Zhong, Z., et al., *NF-kappaB Restricts Inflammasome Activation via Elimination of Damaged Mitochondria.* Cell, 2016. **164**(5): p. 896-910.

55. Wulf, A., et al., *T3-mediated expression of PGC-1alpha via a far upstream located thyroid hormone response element.* Mol Cell Endocrinol, 2008. **287**(1-2): p. 90-5.

56. Ghallab, A., et al., *Model-guided identification of a therapeutic strategy to reduce hyperammonemia in liver diseases.* J Hepatol, 2016. **64**(4): p. 860-71.

57. Sinha, A.K., et al., *Expression pattern of potential biomarker genes related to growth, ion regulation and stress in response to ammonia exposure, food deprivation and exercise in common carp (Cyprinus carpio).* Aquat Toxicol, 2012. **122-123**: p. 93-105.

58. Butterworth, R.F., et al., *Efficacy of l-Ornithine l-Aspartate for the Treatment of Hepatic Encephalopathy and Hyperammonemia in Cirrhosis: Systematic Review and Meta-Analysis of Randomized Controlled Trials.* J Clin Exp Hepatol, 2018. **8**(3): p. 301-313.

59. Karaca, M., et al., *Liver Glutamate Dehydrogenase Controls Whole-Body Energy Partitioning Through Amino Acid-Derived Gluconeogenesis and Ammonia Homeostasis.* Diabetes, 2018. **67**(10): p. 1949-1961.